Journal of Physics: Conference Series **2494** (2023) 012019 doi:10.1088/1742-6596/2494/1/012019

Vacuum Birefringence Measurement via All-Optical Interferometric Schemes

Stefan Ataman

Extreme Light Infrastructure - Nuclear Physics (ELI-NP),
"Horia Hulubei" National R&D Institute for Physics and Nuclear Engineering (IFIN-HH),
30 Reactorului Street, 077125 Bucharest-Măgurele, Romania

E-mail: stefan.ataman@eli-np.ro

Abstract. All-optical vacuum birefringence experiments will get increasingly closer to feasibility as multi-petawatt laser facilities become operational around the World. Thus, the availability of focused laser intensities in the order of $I_L \sim 10^{22} - 10^{24}$ W/cm^2 are to be expected in a focused spot size $\sim 3 - 5\,\mu$m. With these values, vacuum refraction indices in the order of $\Delta n \sim 10^{-11} - 10^{-9}$ are possible with an induced phase delay on a counterpropagating optical probe beam in the order of $\Delta\varphi \sim 10^{-9} - 10^{-7}$ radians. We discuss two all-optical interferometric schemes and detail the Mach-Zender interferometric proposal. We consider this interferometric scheme fed by both classical and non-classical input light and with two detection schemes. We outline scenarios that are likely to lead to a feasible experimental implementation.

1. Introduction

The emergence of pewawatt-class laser facilities [1, 2, 3] opened new perspectives in the research of intense-field QED phenomena [4]. Thus, previously untested QED, as well as BSM (beyond Standard Model), predictions become now closer to experimental verification. Among the still untested QED predictions we mention light-by-light scattering [5, 6], unassisted vacuum pair creation [7] and vacuum birefringence [8]. In this work we will discuss at length the latter.

First considered in [8], the birefringence of the vacuum subjected to an electromagnetic field was soon discussed in terms of a non-linear effectiv electrodynamic theory [9]. When discussing the propagation of a probe photon in a pump-field disturbed vacuum, one can employ an effective nonlinear electrodynamics description [10, 9] or covariant formalisms [11, 12].

For a purely magnetic pump field perpendicular in respect with the probe's propagation direction one has the so-called vacuum Cotton-Mouton effect [13]. Similarly, for a purely electric pump field, one has the vacuum Kerr effect [13]. For a geometry having a probe beam perpendicular on both an electric and magnetic pump fields, equally perpendicular among them, one also finds the magneto-electric vacuum birefringence [14]. For a detailed discussion, see reference [15].

The first class of vacuum birefringence experiments were of Cotton-Mouton type. The PVLAS experiment [16] ran for 40 years with its best sensitivity a factor 50 short of the QED prediction [17]. A similar experiment, BMV [18] is still ongoing.

The emergence of high-power lasers saw new vacuum birefringence measurement proposals [19, 20, 21]. Indeed, the high pump intensities available brought into the realm of possibility

the measurement of polarization flip in a high-energy probe photon [22] either using X-rays [19, 23, 24, 25] or γ-rays [2, 21]. While these high-energy proposals have some advantages (especially the X-ray probes [23]), they also present a number of difficulties.

Another category of experiments propose purely optical vacuum birefingence detection. Initially, a cavity-based [26] proposal was put forward. Taking advantage that optical interferometry is a mature technology, two types of optical interferometric devices have been proposed: a Sagnac-based scheme [27, 28] that aims to detect the tiny displacement cause by the refraction of light in the disturbed vacuum and a Mach-Zehnder based scheme [29] aiming to detect the time delay effect from propagating through the focus of an intense pump laser.

Compared to high-energy probes, all-optical interferometric proposals have a number of advantages. Not only optical components (including detectors) are cheap, low-loss and reliable, but optical interferometry is an old an mature field of science. One can mention in this context the remarkable performance of the graviational wave detectors LIGO [30] and Virgo [31]. Another advantage of optical interferometry is the availability of the technology to go beyond the classical limit, *i. e.* the shot noise limit. Indeed, squeezed light is routinely used [30] and there is an ongoing race towards higher and higher squeezing factors [32].

In this work we focus on all-optical experimental setups that are likely to yield sensitivities in the detection range needed for a vacuum birefringence signal resulting from a PW-class pump laser. We shortly discuss both the Sagnac and Mach-Zehnder interferometer-based proposals while focusing on the latter.

For the Mach-Zehnder interferometer (MZI) we discuss the phase sensitivity both for classical input light leading to the shot-noise limit (SNL) and with non-classical light leading to sub-SNL sensitivities [33, 34, 35, 36]. We also discuss two detection methods, namely the single-mode intensity [37, 38] and the balanced homodyne detection (BHD) schemes [35, 37].

This paper is structured as follows. In Section 2 we briefly introduce the effective theory needed to deduce the vacuum refraction indices for two counter-propagating laser beams and discuss the interaction geometry. In Section 3 we introduce important notions such as the shot-noise limit and the Heisenberg limit and sketch two all-optical vacuum birefringence measurement schemes. A thorough discussion of the MZI scheme is done in Section 4. The paper concludes with the remarks from Section 5.

2. From the Heisenberg-Euler Lagrangian to vacuum birefringence

2.1. The Heisenberg-Euler-Kockel effective Lagrangian

By considering constant or slowly varying electro-magnetic fields, one can integrate out the fermionic degrees of freedom from the QED Lagrangian and arrive at the effective theory described by the Heisenberg-Euler (HE) Lagrangian [7, 13, 39]. Since current laboratory-based fields obey $|\boldsymbol{E}| \ll E_S$ and $|\boldsymbol{B}| \ll B_S$ where the critical fields [40] are defined as usual by $E_S = m^2c^3/e\hbar$ and $B_S = E_S/c$, performing a lowest order expansion of the HE Lagrangian brings us to the so-called Heisenberg-Euler-Kockel or Euler-Kockel (EK) [13, 41, 42] Lagrangian,

$$\mathcal{L}_{EK} = \frac{\mathcal{F}}{2} + \Lambda_{EK}\left(\mathcal{F}^2 + 7\mathcal{G}^2\right) \tag{1}$$

where we have the constant

$$\Lambda_{EK} = \frac{\alpha}{90\pi\varepsilon_0 E_S^2} = \frac{\alpha\mu_0}{90\pi B_S^2} = \frac{2\alpha^2\hbar^3}{45m^4c^5} = \frac{\hbar e^4}{360\pi^2\varepsilon_0^2 m^4 c^7} \approx 1.65\times10^{-30} \quad \left[\frac{\mathrm{m}^3}{\mathrm{J}}\right]. \tag{2}$$

In the previous equations e (m) denotes the charge (mass) of the electron, h ($\hbar = h/2\pi$) is the (reduced) Planck constant and the QED fine-structure constant is defined, as usual by $\alpha = e^2/4\pi\varepsilon_0\hbar c \approx 1/137$. For a compact writing of equation (1) we also introduced the two invariants of the electromagnetic field $\mathcal{F} = \epsilon_0\left(E^2 - c^2B^2\right)$ and $\mathcal{G} = \sqrt{\varepsilon_0/\mu_0}\boldsymbol{E}\cdot\boldsymbol{B}$.

2.2. Refraction indices in a vacuum disturbed by a strong laser field

We assume a geometry with two counter-propagating linearly polarized laser beams, namely a probe field having $\boldsymbol{E}_p = E_p\hat{\boldsymbol{x}}$ ($\boldsymbol{B}_p = B_p\hat{\boldsymbol{y}}$), propagating along the positive z-axis and a much stronger pump laser propagating along the negative z-axis. In the "$\parallel$" scenario we have $\boldsymbol{E}_L = E_L\hat{\boldsymbol{x}}$, while in the "$\perp$" scenario we have $\boldsymbol{E}_L = E_L\hat{\boldsymbol{y}}$, see Fig. 1. We assume both the pump and the probe to be nearly monochromatic.

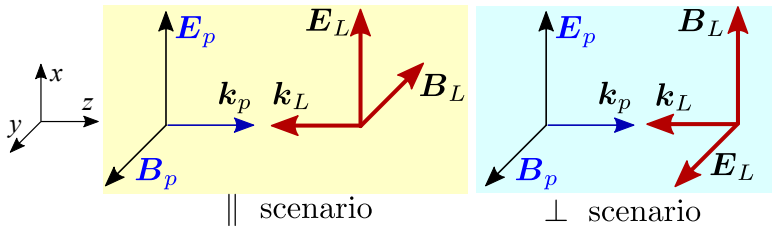

Figure 1. The collision geometry of the pump and probe laser beams.

If we assume the "$\parallel$" geometry ($\boldsymbol{E}_L \parallel \boldsymbol{E}_p$, $\boldsymbol{B}_L \parallel -\boldsymbol{B}_p$), the probe beam propagating in the pump-disturbed vacuum, will see a refraction index[1] [8, 19, 42]

$$n_{\parallel} = 1 + 16\varepsilon_0\Lambda_{EK}E_L^2 = 1 + 32\Lambda_{EK}\frac{I_L}{c} \tag{3}$$

where we assumed $E_L = cB_L$ and the intensity of the pump beam is taken[2] $I_L = c\varepsilon_0 E_L^2/2$. If we assume the "$\perp$" geometry (hence $\boldsymbol{E}_L \perp \boldsymbol{E}_p$ and $\boldsymbol{B}_L \perp \boldsymbol{B}_p$), the probe beam propagating in the pump-disturbed vacuum will see a higher refraction index, namely

$$n_{\perp} = 1 + 28\varepsilon_0\Lambda_{EK}E_L^2 = 1 + 56\Lambda_{EK}\frac{I_L}{c}. \tag{4}$$

The difference $n_{\perp} - n_{\parallel}$ yields the vacuum birefringence, $\Delta n = 24\Lambda_{EK}I_L/c$. We display the expected vacuum refraction indices for some values of the focused pump field in Table 1.

Table 1. Expected vacuum refraction indices versus the focused pump laser intensity.

Focused pump laser intensity I_L [W/cm^2]	"$\perp$" refraction index, $\Delta n_{\perp} = n_{\perp} - 1$	"$\parallel$" refraction index, $\Delta n_{\parallel} = n_{\parallel} - 1$	vacuum birefringence, $\Delta n = n_{\perp} - n_{\parallel}$
10^{22}	3.08×10^{-11}	1.76×10^{-11}	1.32×10^{-11}
10^{23}	3.08×10^{-10}	1.76×10^{-10}	1.32×10^{-10}
10^{24}	3.08×10^{-9}	1.76×10^{-9}	1.32×10^{-9}

[1] For a detailed deduction of the results from equations (3) and (4) see reference [15].

[2] We assume the pump field to be monochromatic, the intensity is thus connected to its "effective" value $E_L/\sqrt{2}$, hence the factor of 2 taken in our definition of I_L.

2.3. The probe beam's propagation in the pump-perturbed vacuum

As discussed in Section 2.2, a probe beam (counter-)propagating through the focus of a strong pump beam is behaving as if it would propagate through a material medium with a refraction index $n > 1$. For the two collision geometries described in Fig. 1, the refraction index is either $n_{\parallel}$ given by equation (3) or $n_{\perp}$ given by equation (4). Assuming that we have a Gaussian pump beam, the beam width $w(z)$ varies longitudinally from the focus point (assumed at $z = 0$) as $w(z) = w_0\sqrt{1 + z^2/z_R^2}$ where the Rayleigh distance z_R is defined as usual by $z_R = \pi w_0^2/\lambda_L$ and throughout this work we will assume a pump central wavelength of $\lambda_L = 800$ nm. We can thus approximate the pump's intensity to its maximum value I_L over a length $b = 2z_R$ (usually called depth of focus), see Fig. 2. Since the typical focused waists are in the order of $w_0 \approx 3 - 5\ \mu$m, we expect a parameter $b \approx 70 - 200\ \mu$m. We will use this fact in Section 3.1. Assuming the pump laser to have a pulse duration in the range $\tau_L \approx 25 - 30$ fs [2, 3], the relevant longitudinal interaction region is $z_{int} = c\tau_L \approx 7.5 - 9\ \mu$m. The counterpropagating probe beam will thus accumulate a phase $\varphi_{\perp/\parallel} = \omega_p z_{int} n_{\perp/\parallel}/c$ where $\omega_p = 2\pi c/\lambda_p$ is the probe (angular) frequency and λ_p denotes its wavelength. We thus expect the relative phase delays in an interferometer

$$\left\{ \begin{array}{c} \Delta\varphi_{\perp} \\ \Delta\varphi_{\parallel} \end{array} \right\} = \frac{2\pi\tau_L \Lambda_{EK}}{\lambda_p} \times \left\{ \begin{array}{c} 56 \\ 32 \end{array} \right\} \times I_L. \tag{5}$$

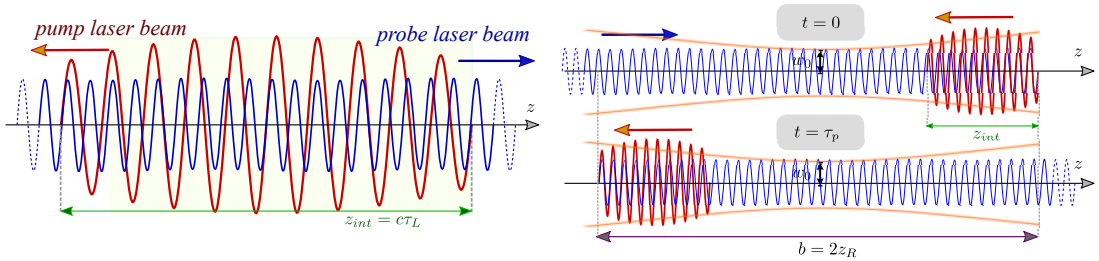

Figure 2. Symbolic representation of the pump-probe interaction geometry (left). The probe beam has a longer pulse duration, $\tau_p \approx b/c$, where $b = 2z_R$ and z_R is the Rayleigh length. (right) The orange cuve symbolically depicts the pump width variation in the depth of focus.

In Table 2 we detail the expected phase shifts for a number of focused intensities. We conclude that the range of expected vacuum birefringence induced phase shifts is in the order of $10^{-9} - 10^{-7}$ radians. These estimations are based on the pulse duration of the ELI-NP lasers [2, 3]. If one considers the upcoming ELI Beamlines L4 Aton laser (10 PW, 1.5 kJ/pulse) featuring a pulse duration of $\tau_L = 150$ fs, one needs to multiply by a factor of ~ 6 all results from Table 2, leading to a much more optimistic range of induced phase shifts in the order of $10^{-8} - 10^{-6}$ radians.

3. All-optical interferometric schemes to measure vacuum birefringence

3.1. The shot-noise limit, the Heisenberg limit and the minimum needed probe laser peak power

It is well known that if one uses classical input light, we have a shot-noise limited (sometimes called Poisson limited) phase sensitivity in an interferometer $\Delta\varphi_{SNL} = 1/\sqrt{\langle N\rangle}$ [43, 34] where $\langle N\rangle$ denotes the average number of input photons. Thus, given a target phase sensitivity $\Delta\varphi_{\perp/\parallel}$ to be attained, we need a minimum average number of photons $\langle N\rangle_{min} \geq 1/\left(\Delta\varphi_{\perp/\parallel}\right)^2$. If we assume a target phase sensitivity in the order $\mathcal{O}(10^{-8})$, this implies a shot-noise limited minimum

Table 2. Expected phase shifts versus the focused pump intensity.

Focused pump laser intensity I_L [W/cm^2]	Induced phase shift $\Delta\varphi_\perp$ [radians]	Induced phase shift $\Delta\varphi_\parallel$ [radians]
10^{22}	2.73×10^{-9}	1.56×10^{-9}
10^{23}	2.73×10^{-8}	1.56×10^{-8}
10^{24}	2.73×10^{-7}	1.56×10^{-7}

number of photons for successful detection of $\langle N\rangle_{min} = \mathcal{O}(10^{16})$. Assuming that the probe laser has a pulse duration of τ_p, the average number of probe photons during the interaction time is $\langle N\rangle_{probe} = P_p\tau_p/\hbar\omega_p = P_p\tau_p\lambda_p/hc$. We can thus estimate the needed probe power in order to be able to detect the QED induced phase shifts by replacing $\langle N\rangle_{min}$ with $\langle N\rangle_{probe}$. We find

$$P_p \geq \frac{hc}{\tau_p\lambda_p}\frac{1}{\left(\Delta\varphi_{\perp/\parallel}\right)^2}. \tag{6}$$

The only variable yet to be determined in the RHS of the previous equation is the probe pulse duration (τ_p). If we assume a counter-propagating geometry, as detailed in Fig. 2 (right) the ideal probe pulse duration should obey $c\tau_p \sim b$, we thus take $\tau_p = 2z_R/c$. Indeed, while counter-propagating, one can take advantage of the slow variation of the pump waist in the interval $[-z_R, z_R]$. For the expected range of focused pump waist $w_0 \approx 3 - 5\,\mu$m we thus get the ideal probe pulse duration $\tau_p \approx 235 - 654$ fs.

The fact that $\tau_p \gg \tau_L$ has a number of positive side-effects. Besides the fact that more probe photons participate in the interaction and thus a lower power is needed, the longer probe pulse ($\sim$ ns range) is positive both from an optical and electronic/detection point of view.

Plugging the values from Table 2 into equation (6) and assuming a pump pulse duration $\tau_L \approx 25 - 30$ fs implies a required probe laser power in the range $P_p \sim 2$ GW $-$ 20 TW. These peak powers for femtosecond-nanosecond pulsed lasers are readily available today.

One can however, use non-classical states of light and thus the shot-noise limit $\Delta\varphi_{SNL}$ can be surpassed. The theoretical best case limit is the so-called Heisenberg limit $\Delta\varphi_{HL} = 1/\langle N\rangle$ [34, 43]. If, similar to reference [42], we consider this limit and a target phase sensitivity in the order $\mathcal{O}(10^{-8})$, it implies a Heisenberg limited number of photons $\langle N\rangle_{min} = \mathcal{O}(10^8)$. For the current experiment, though, this scenario is not realistic and is of purely theoretical interest. However, there are intermediate sub-SNL phase sensitivities $\Delta\varphi_{HL} \leq \Delta\varphi_{sub-SNL} \leq \Delta\varphi_{SNL}$ that are feasible, a good example being the coherent plus squeezed vacuum input [33], the very input state that boosed LIGO's sensitivty [30].

3.2. Sagnac-based interferometric scheme

A Sagnac interferometer can be used in an all-optical vacuum birefringence scheme[3] [28], as depicted in Fig. 3. The balanced beam splitter (denoted BS_1) splits the input pulse into a reference and a probe one. By reference we understand the pulse that will not meet head-on and counter-propagating the pump laser in its focus depth. On the contrary, the probe pulse will meet the pump beam exactly in the "hot spot", as depicted in Fig. 3. Thus, assuming that the pump laser is off, no signal is expected at the output port 3 (*i. e.* "dark port"). Assuming now that the pump laser is on, the two beams will collide in the geometry described in Fig. 2,

[3] In reference [28], although a phase delay effect takes place, the authors intend to measure the minute displacement of the intensity profile in the dark port ($\Delta y \sim 13$ pm) caused by the refraction of the probe beam while propagating through the pump-disturbed vacuum.

creating a delay in respect with the reference beam and thus generating a signal in the output port 3.

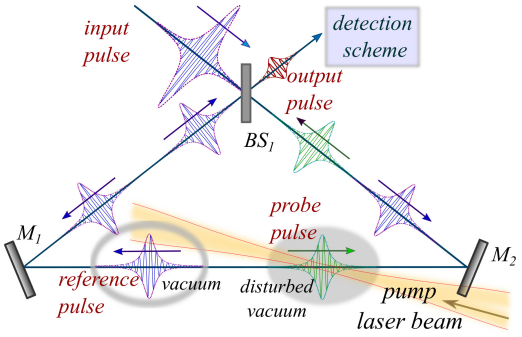

Figure 3. Sagnac-based all-optical vacuum birefringence interferometric detection setup. See main text for details.

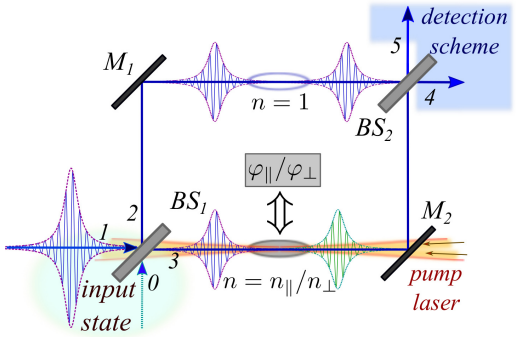

Figure 4. Mach-Zehnder based all-optical vacuum birefringence measurement setup. See main text for details.

3.3. Mach-Zehnder based interferometric scheme

In Fig. 4 we depict a Mach-Zehnder based interferometric scheme [29]. We consider the same pump-probe geometry from Fig. 2, with the pump-disturbed vacuum (depicted as a gray blob). Hence, a laser pulse propagating inside the interferometer will be slightly delayed in the lower arm. This delay can be detected at the output.

4. Detailed discussion of a Mach-Zehnder interferometer-based proposal

From a quantum optical point of view, a Sagnac interferometer ca be seen as a "folded" MZI. We can thus discuss only the latter, the conclusions applying to both interferometric schemes. Throughout this section we assume the MZI input state (denoted by $|\psi_{in}\rangle$) to be pure.

4.1. MZI phase sensitivity with classical input states

The phase sensitivity of a MZI has been studied at length in the literature [35, 36, 37, 38, 44]. Taking into account that our scenario involves high peak powers, some detection schemes are more suited. We thus consider the single-mode intensity detection[4] and the BHD[5] schemes (see Fig. 5). This time we split the internal phase shift into two components, the tiny QED-induced phase shift φ_s and the experimentally controllable ϕ so that $\varphi = \varphi_s + \phi$. As we will discuss shortly, for each considered input state/detection scheme, by adjusting ϕ to ϕ_{opt} we can put the MZI in its optimum working point (also called "sweet spot").

The first input we consider is a coherent (plus vacuum) state,

$$|\psi_{in}\rangle = \hat{D}_1(\alpha)|0\rangle = |\alpha_1 0_0\rangle \tag{7}$$

where $|0\rangle$ denotes the vacuum, $\alpha = |\alpha|e^{i\theta_\alpha}$, θ_α denotes the phase of the coherent source and the displacement operator is defined by $\hat{D}_1(\alpha) = e^{\alpha\hat{a}_1^\dagger - \alpha^*\hat{a}_1}$ [44]. Throughout this work $\hat{a}_m^\dagger/\hat{a}_m$

[4] This detection scheme features a photo-detector placed at one MZI output port (output 4 in our case). The operator modelling this scheme is $\hat{n}_4$. For a detailed discussion of this detection scheme see references [35, 37, 38].
[5] The BHD scheme mixes the output of port 4 with a stong coherent source ("local oscillator") $|\gamma_L\rangle$ where $\gamma_L = |\gamma_L|e^{i\phi_L}$. The operator modelling this detection scheme is $\hat{X}_{\phi_L} = 1/2(\hat{a}_4 e^{-i\phi_L} + \hat{a}_4^\dagger e^{i\phi_L})$. For more details on this detection scheme see references [35, 37, 45].

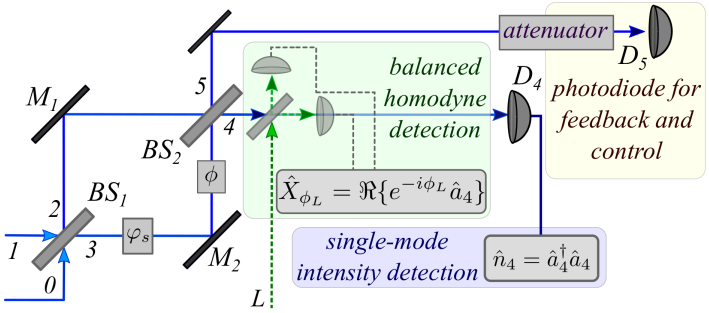

Figure 5. The Mach-Zehnder interferometer with the two considered detection schemes, namely the single mode intensity (modelled via the operator $\hat{n}_4$) and BHD (modelled via the operator $\hat{X}_{\phi_L}$). The QED-induced phase shift is modeled via the phase shift φ_s.

represent the creation/annihilation operators for mode m. The average number of photons for the input state (7) is given by $\langle N\rangle = \langle \hat{n}_1\rangle = |\alpha|^2$ where $\hat{n}_k$ denotes the photon number operator for mode k. Both beam splitters are assumed balanced, we thus have the transmission (reflection) coefficients $T = T' = 1/\sqrt{2}$ ($R = R' = i/\sqrt{2}$) [44]. There exists a theoretical optimum bound, derived from purely quantum estimation theory, called the quantum Cramér-Rao bound (QCRB), itself implied by the quantum Fisher information (see Appendix A). For a MZI featuring the input state (7) one finds that the theoretical best phase sensitivity is given by [38, 46]

$$\Delta\varphi_{QCRB} = \frac{1}{|\alpha|}. \tag{8}$$

Incidentally, in this case this is also the shot-noise limit. The phase sensitivity of a MZI with single-mode intensity detection [37, 38] is found to be $\Delta\varphi_{sg} = 1/|\alpha \sin(\varphi/2)|$ the optimum working point being obviously $\phi_{opt} = \pi$. For a BHD scheme, the phase sensitivity is given by $\Delta\varphi_{hom} = 1/|\alpha\cos\varphi|$ [35, 37]. In Fig. 6 we depict the phase sensitivity for a coherent input state for $|\alpha| = 10^8$ (this corresponds to $P \approx 15.9$ TW if we assume $\tau_p \approx 235$ fs). Both considered detection schemes yield the same working point around $\phi_{opt} = \pi$, where they reach the QCRB (horizontal thick dotted green line), proof that they are optimal.

4.2. MZI phase sensitivity with non-classical input states

As mentioned in Section 3.1, the shot-noise limit can be surpassed by employing non-classical states of light. One such state is the coherent plus squeezed vacuum input [33, 47],

$$|\psi_{in}\rangle = \hat{D}_1(\alpha)\,\hat{S}_0(\xi)\,|0\rangle = |\alpha_1\xi_0\rangle \tag{9}$$

where the squeezing operator is $\hat{S}_0(\xi) = e^{1/2[\xi^*\hat{a}_0^2 - \xi(\hat{a}_0^\dagger)^2]}$ [44]. Here $\xi = re^{i\theta}$, $r \in \mathbb{R}^+$ is called the squeezing factor and θ denotes the phase of the squeezed state. The average number of photons of the coherent plus squeezed vacuum input state is $\langle N\rangle_{csv} = |\alpha|^2 + \sinh^2 r$. The optimum input phase matching condition (PMC) imposes $2\theta_\alpha - \theta = 0$ [35, 36]. The theoretical optimum phase sensitivity provided by the QCRB is found to be $\Delta\varphi_{QCRB} = 1/\sqrt{|\alpha|^2 e^{2r} + \sinh^2 r}$ [36]. A Heisenberg scaling is possible if we impose $|\alpha|^2 \approx \sinh^2 r$ [36] *i. e.* we put the same amount of energy in the coherent state and in the squeezed vacuum. However, in a realistic setup the coherent source will be much stronger than the squeezed vacuum *i. e.* $|\alpha|^2 \gg \sinh^2 r$ the QCRB can thus be approximated as

$$\Delta\varphi_{QCRB} \simeq \frac{e^{-r}}{|\alpha|}. \tag{10}$$

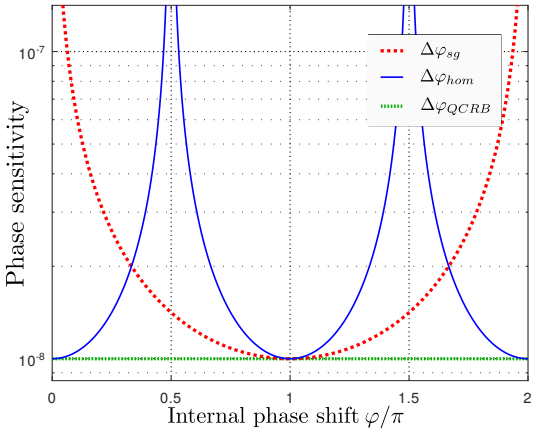

Figure 6. Phase sensitivity for a MZI with a coherent input state. Parameter used: $|\alpha| = 10^8$.

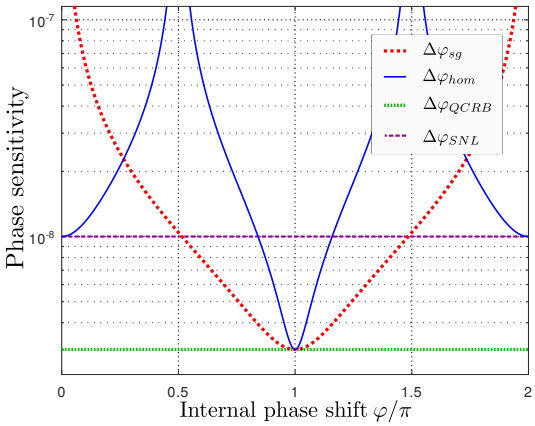

Figure 7. Phase sensitivity for a MZI with the input state (9). Parameters used: $|\alpha| = 10^8$, $2\theta_\alpha - \theta = 0$, and $r = 1.2$.

For a single-mode intensity detection scheme we have $\phi_{opt} \approx \pi$ [38, 47]. The optimum phase sensitivity is given in reference [38], equation (38). In the high-coherent regime it can be approximated to $\Delta\varphi_{sg} = e^{-r}/|\alpha|$ and this is indeed the QCRB from equation (10). For a BHD scheme the optimum working point is $\phi_{opt} = \pi$ [35, 37] and at this point we again find $\Delta\varphi_{hom} = e^{-r}/|\alpha|$.

In Fig. 7 we depict the phase sensitivity performance of a coherent plus squeezed vacuum input (9) with a squeezing factor $r = 1.2$ (≈ 10 dB). Similar to the discussion from Fig. 6, both detection schemes have their optimum working points around $\phi_{opt} = \pi$ and their performance is almost optimal. The horizontal thick dotted green line represents the QCRB while the horizontal dashed magenta line represents the SNL, $\Delta\varphi_{SNL} = 1/\sqrt{\langle N\rangle_{csv}}$. The latter is the theoretical limit when using classical input states [34]. As seen from Fig. 7, we go beyond this limit, hence we are in the sub-shot noise (*i. e.* non-classical) regime. Compared to the best performance from Fig. 6, the gain is close to a factor of 3, as predicted by equation (10). We would like to point out that this improvement was done by using only an average number of $\sinh^2 r \approx 2.3$ squeezed photons, despite the fact that the coherent source has an average of $|\alpha|^2 = 10^{16}$ photons.

4.3. Practical considerations for a MZI implementation

While a detailed discussion of the practical experimental setup including all non-idealities goes beyond the scope of this paper and will be the subject of a future work, we can briefly consider a number of factors that will influence the expected phase sensitivity in a real-life implementation.

When considering the effect of losses, it is well known that for a coherent input they can be modelled by replacing $\alpha \to \sqrt{1-\sigma}\alpha$ [48] where $\sigma \in [0, 1]$ models the amount of losses, $\sigma = 0$ being the lossless case. Thus, the optimum expected phase sensitivity changes from the value given in equation (8) to $\Delta\varphi_{QCRB,l} = 1/\sqrt{1-\sigma}|\alpha|$. We do not expect this effect to be important for classical input light. Also, the probe laser being pulsed, it is actually a multi-mode coherent state, featuring a central frequency ω_p and a spectral width $\Delta\omega_p$. Thus, in respect with the plane-wave SNL we assumed here, we expect a phase sensitivity $\Delta\varphi_{pulsed} \approx \Delta\varphi_{SNL}/\sqrt{\Delta\omega_p^2/\omega_p^2 + 1}$. However, considering that the probe laser has its optimum pulse duration τ_p in the ns range, the ratio $\Delta\omega_p^2/\omega_p^2$ is negligible compared to 1.

4.4. Other techniques likely to yield an improved phase sensitivity

In this short section we mention more speculative ideas that might provide an improved phase sensitivity in respect with the already discussed cases. If one allows the MZI to be unbalanced [45, 49], a detection scheme having access to an external phase reference could provide an improvement in its theoretical phase sensitivity [45, 50, 51] (see also Appendix A). This effect is still valid in the high-coherent regime [45, 51].

Another interesting evolution could be the addition of OAM (orbital angular momentum, also called optical angular momentum) [52]. Recently, descriptions of Laguerre-Gauss beams [53, 54] have been reported. By employing OAM (*e. g.* $l = 1$ for the pump beam and no OAM $l = 0$ to the probe beam) could allow a better filtering of the unwanted stray photons at the detection site, potentially minimizing the need to use a different wavelength for the probe beam.

5. Conclusion

In this work we discussed all-optical interferometric schemes that could potentially measure the vacuum birefringence signal induced by a strong, counter-propagating pump laser. If we optimally exploit the counter-propagating collision geometry of the two lasers, the ideal pulse duration of the probe beam should match the depth of focus of the pump laser.

Since from a quantum optical point of view both the Sagnac and Mach-Zehnder interferometers are equivalent, we discussed in detail the latter. We considered both classical and non-classical input states and evaluated the expected phase sensitivity.

Given the new petawatt laser facilities that started operating (or will be available in the near future), the all-optical vacuum birefringence measurement scheme seems a promising candidate in the list of possible experiments.

Acknowledgments

The Author would like to thank Dr. Cesim K. Dumlu for reading this manuscript and providing feedback. It is acknowledged that this research was supported from the Nucleu Project, PN 19 06 01 05. It is also acknowledged that this work has been supported by the Extreme Light Infrastructure Nuclear Physics (ELI-NP) Phase II, a project co-financed by the Romanian Government and the European Union through the European Regional Development Fund and the Competitiveness Operational Programme (1/07.07.2016, COP, ID 1334).

Appendix A. Quantum Fisher information and the quantum Cramér-Rao bound

When dealing with a single parameter estimation, the optimal solution is found by employing the quantum Fisher information (QFI) [55]. Indeed, from the QFI one can infer the minimum variance for the esimation of a parameter [34, 55]. As discussed in the literature [46], applying the single parameter QFI to a MZI yields over-optimistic results due to counting resources that are not necessarily available. If one implements a detection scheme not having access to an external phase reference, then in order not to obtain over-optimistic results, one has to do one of the following: i) average out the input state in respect with a common phase or ii) use the two-parameter QFI. We chose the latter in this work.

Thus, when dealing with a multi-parameter estimation problem the single QFI approach has to be extended to a matrix form [45, 46, 56]. We replace the QFI by a 2×2 matrix having the Fisher matrix elements, $\mathcal{F}_{ij} = 4\Re\{\langle\partial_i\psi|\partial_j\psi\rangle - \langle\partial_i\psi|\psi\rangle\langle\psi|\partial_j\psi\rangle\}$ [46, 56] with $i, j \in \{s, d\}$ and we performed the variable changes $\varphi_s = \varphi_1 + \varphi_2$ and $\varphi_d = \varphi_1 - \varphi_2$. The quantum Cramér-Rao bound implies the matrix inequality $\mathbf{\Sigma} \geq \boldsymbol{\mathcal{F}}^{-1}$ [56, 57] (see also equation (A3) in [51]). We will saturate only the inequality corresponding the difference-difference phase estimator, we thus introduce the definition $\mathcal{F}^{(2p)} = \mathcal{F}_{dd} - \mathcal{F}_{sd}^2/\mathcal{F}_{ss}$ [45]. Thus, throughout this work we will use the QCRB, $\Delta\varphi_{QCRB} = 1/\sqrt{\mathcal{F}^{(2p)}}$. Nevertheless, if one uses a detection scheme having access to an external phase (*e. g.* BHD), then the two-parameter QFI can be surpassed [45, 46, 50].

References

[1] Sung J H *et al.* 2017 *Opt. Lett.* **42** 2058–2061
[2] Galès S *et al.* 2018 *Reports on Progress in Physics* **81** 094301
[3] Lureau F *et al.* 2020 *High Power Laser Science and Engineering* **8** e43
[4] Di Piazza A, Müller C, Hatsagortsyan K Z and Keitel C H 2012 *Rev. Mod. Phys.* **84** 1177–1228
[5] Halpern O 1933 *Phys. Rev.* **44** 855–856
[6] Costantini V, De Tollis B and Pistoni G 1971 *Nuov Cim A* **2** 733
[7] Schwinger J 1951 *Phys. Rev.* **82** 664–679
[8] Klein J J and Nigam B P 1964 *Phys. Rev.* **135** B1279
[9] Bialynicka-Birula Z and Bialynicki-Birula I 1970 *Phys. Rev. D* **2** 2341–2345
[10] Aleksandrov E B, Ansel'm A A and Moskalev A N 1985 *JETP* **62** 680
[11] Karbstein F and Shaisultanov R 2015 *Phys. Rev. D* **91** 085027
[12] Karbstein F and Shaisultanov R 2015 *Phys. Rev. D* **91** 113002
[13] Battesti R and Rizzo C 2013 *Reports on Progress in Physics* **76** 016401
[14] Rikken G L J A and Rizzo C 2000 *Phys. Rev. A* **63** 012107
[15] Dittrich W and Gies H 2000 *Probing the Quantum Vacuum. Pertubative Effective Action Approach in Quantum Electrodynamics and its Application* (Springer)
[16] Della Valle F *et al.* 2016 *Eur. Phys. J. C* **76** 24
[17] Ejlli A *et al.* 2020 *Physics Reports* **871** 1
[18] Cadène A, Berceau P, Fouché M, Battesti R and Rizzo C 2014 *Eur. Phys. J. D* **68** 16
[19] Heinzl T, Liesfeld B, Amthor K U, Schwoerer H, Sauerbrey R and Wipf A 2006 *Opt. Comm.* **267** 318
[20] King B and Heinzl T 2016 *High Power Laser Science and Engineering* **4** e5
[21] Nakamiya Y and Homma K 2017 *Phys. Rev. D* **96** 053002
[22] Dinu V, Heinzl T, Ilderton A, Marklund M and Torgrimsson G 2014 *Phys. Rev. D* **89** 125003
[23] Schlenvoigt H P, Heinzl T, Schramm U, Cowan T E and Sauerbrey R 2016 *Physica Scripta* **91** 023010
[24] Karbstein F and Sundqvist C 2016 *Phys. Rev. D* **94** 013004
[25] Karbstein F 2018 *Phys. Rev. D* **98** 056010
[26] Luiten A N and Petersen J C 2004 *Phys. Lett. A* **330** 429
[27] Sarazin X *et al.* 2016 *Eur. Phys. J. D* **70** 13
[28] Robertson S *et al.* 2021 *Phys. Rev. A* **103** 023524
[29] Ataman S 2018 *Phys. Rev. A* **97** 063811
[30] Tse M *et al.* 2019 *Phys. Rev. Lett.* **123** 231107
[31] Abbott B P *et al.* 2020 *Living Reviews in Relativity* **23** 3
[32] Schnabel R 2017 *Physics Reports* **684** 1 – 51
[33] Caves C M 1981 *Phys. Rev. D* **23** 1693–1708
[34] Paris M G A 2009 *International Journal of Quantum Information* **07** 125–137
[35] Ataman S 2019 *Phys. Rev. A* **100** 063821
[36] Pezzé L, Smerzi A, Khoury G, Hodelin J F and Bouwmeester D 2007 *Phys. Rev. Lett.* **99** 223602
[37] Gard B T, You C, Mishra D *et al.* 2017 *EPJ Quantum Technology* **4** 4
[38] Ataman S, Preda A and Ionicioiu R 2018 *Phys. Rev. A* **98** 043856
[39] Heisenberg W and Euler H 1936 *Z. Physik* **98** 714–732
[40] Sauter F 1931 *Z. Physik* **69** 742–764
[41] Euler H and Kockel B 1935 *Naturwissenschaften* **23** 246–247
[42] Ahmadiniaz N *et al.* 2020 *Phys. Rev. D* **101** 116019
[43] Giovannetti V, Lloyd S and Maccone L 2006 *Phys. Rev. Lett.* **96** 010401
[44] Gerry C and Knight P 2005 *Introductory Quantum Optics* (Cambridge University Press)
[45] Ataman S 2020 *Phys. Rev. A* **102** 013704
[46] Jarzyna M and Demkowicz-Dobrzański R 2012 *Phys. Rev. A* **85** 011801(R)
[47] Pezzé L and Smerzi A 2008 *Phys. Rev. Lett.* **100** 073601
[48] Ono T and Hofmann H F 2010 *Phys. Rev. A* **81** 033819
[49] Preda A and Ataman S 2019 *Phys. Rev. A* **99** 053810
[50] Ataman S 2022 *Phys. Rev. A* **105** 012604
[51] Mishra K K and Ataman S 2022 *Phys. Rev. A* **106** 023716
[52] Allen L, Beijersbergen M W, Spreeuw R J C and Woerdman J P 1992 *Phys. Rev. A* **45** 8185–8189
[53] Karbstein F and Mosman E A 2017 *Phys. Rev. D* **96** 116004
[54] Dumlu C K, Nakamiya Y and Tanaka K A 2022 *Phys. Rev. D* **106** 116001
[55] Helstrom C 1967 *Phy. Lett. A* **25** 101–102
[56] Lang M D and Caves C M 2013 *Phys. Rev. Lett.* **111** 173601
[57] Pezzè L, Hyllus P and Smerzi A 2015 *Phys. Rev. A* **91** 032103